PHYSICAL REVIEW B **89**, 245428 (2014)

Structure and dynamics of C_{60} molecules on Au(111)

Heekeun Shin, A. Schwarze, and R. D. Diehl
Department of Physics, Penn State University, University Park, Pennsylvania 16802, USA

K. Pussi
Department of Mathematics and Physics, Lappeenranta University of Technology, P.O. Box 20, FIN-53851 Lappeenranta, Finland

A. Colombier, É. Gaudry, J. Ledieu, G. M. McGuirk, L. N. Serkovic Loli, and V. Fournée
Institut Jean Lamour, UMR 7198 CNRS-Université de Lorraine, Parc de Saurupt, CS50840, F-54011 Nancy Cedex, France

L. L. Wang
Division of Materials Science and Engineering, Ames Laboratory, U.S. Department of Energy, Ames, Iowa 50011, USA

G. Schull
Institut de Physique et Chimie des Matériaux de Strasbourg, UMR 7504 (CNRS, Université de Strasbourg), 67034 Strasbourg, France

R. Berndt
Institut fur Experimentelle und Angewandte Physik, Christian-Albrechts-Universitt zu Kiel, D-24098 Kiel, Germany
(Received 21 March 2014; revised manuscript received 3 June 2014; published 19 June 2014)

Earlier studies of C_{60} adsorption on Au(111) reported many interesting and complex features. We have performed coordinated low-energy electron diffraction, scanning tunneling microscopy (STM), and density functional theory studies to elucidate some of the details of the monolayer commensurate $(2\sqrt{3} \times 2\sqrt{3})$R30° phase. We have identified the adsorption geometries of the two states that image as dim and bright in STM. These consist of a C_{60} molecule with a hexagon side down in a vacancy (hex-vac) and a C_{60} molecule with a carbon-carbon 6:6 bond down on a top site (6:6-top), respectively. We have studied the detailed geometries of these states and find that there is little distortion of the C_{60} molecules, but there is a rearrangement of the substrate near the C_{60} molecules. The two types of molecules differ in height, by about 0.7 Å, which accounts for most of the difference in their contrast in the STM images. The monolayer displays dynamical behavior, in which the molecules flip from bright to dim, and vice versa. We interpret this flipping as the result of the diffusion of vacancies in the surface layers of the substrate. Our measurements of the dynamics of this flipping from one state to the other indicate that the activation energy is 0.66 ± 0.03 eV for flips that involve nearest-neighbor C_{60} molecules, and 0.93 ± 0.03 for more distant flips. Based on calculated activation energies for vacancies diffusing in Au, we interpret these to be a result of surface vacancy diffusion and bulk vacancy diffusion. These results are compared to the similar system of Ag(111)-$(2\sqrt{3} \times 2\sqrt{3})$R30°-$C_{60}$. In both systems, the formation of the commensurate C_{60} monolayer produces a large number of vacancies in the top substrate layer that are highly mobile, effectively melting the interfacial metal layer at temperatures well below their normal melting temperatures.

DOI: 10.1103/PhysRevB.89.245428 PACS number(s): 68.43.Fg, 68.37.Ef, 68.35.bp

I. INTRODUCTION

The growth and structures of C_{60} films on Au(111) surfaces have been studied extensively [1–27]. Early scanning tunneling microscopy (STM) studies at room temperature (RT) on Au(111) produced images of well-ordered close-packed lattices of C_{60} molecules having an intermolecular spacing very close to the C_{60} bulk spacing, but having domains of different lattice orientations [1,3,8,9,13]. (In this paper, the 0° orientation refers to an alignment of the C_{60} lattice with the substrate lattice.) Low-energy electron diffraction (LEED) [22], surface x-ray diffraction (SXRD), [28] and STM [2,16,17] measurements have shown that these hexagonal compact structures on Au(111) have essentially three different superlattices, $(2\sqrt{3} \times 2\sqrt{3})$R30°, (7×7)R0°, and $(\sqrt{589} \times \sqrt{589})$R14.5°, which contain 1, 4, and 49 molecules per unit cell, respectively. Annealing the surface after dosing resulted in growth of domains having lattices oriented at 30° at the expense of the other orientations. Those domains were verified to correspond to the commensurate $(2\sqrt{3} \times 2\sqrt{3})$R30° structure [2,9] and it was concluded that this was the stable structure of the monolayer. A more recent SXRD study analyzed the adsorption geometry of the C_{60} on Au(111) in this commensurate structure and found that at room temperature, the best fit is obtained for a model in which the C_{60} molecules adsorb on single-atom vacancies at a height of 1.986 ± 0.14 Å and C-Au bond lengths of 2.49 ± 0.1 Å [27].

It was observed in the STM studies that bright and dim contrast molecules coexist in some of the surface phases [15], appearing as either "quasiperiodic" (meaning almost periodic) or "disordered" in the different structural domains. High annealing temperatures (~400 °C) produced mainly "disordered" domains, identified as the stable $(2\sqrt{3} \times 2\sqrt{3})$R30° structure [15]. Flipping of the molecules from bright to dim contrast, and vice versa, was observed in both types of domains

at room temperature, but no flipping was observed at 77 K [15]. A similar situation was observed and studied for C_{60} on Ag(111) [29]. On Au(111), the proportion of bright molecules is about 40% at room temperature [15]. High-resolution STM images at room temperature helped to discern intramolecular features that suggest that the dim molecules are hexagon down (hex) [15], and it was inferred that the bright-dim contrast may arise partly from a real height difference between the C_{60} molecules, possibly due to some C_{60} sitting in nanopits (substrate vacancies), and partly from a difference in electronic structure related to molecular distortion [15]. STM images taken at 5 K showed even clearer evidence that the dim molecules are hex, and that the bright ones are oriented with their 6:6 carbon bonds down with their molecular mirror planes parallel to the substrate mirror planes and a slight tilt in the C-C bond [18].

In order to gain more information about the mixed bright-dim domains, we have extended the analysis of low-temperature STM data in order to elucidate more structural details, and we have performed low-energy electron diffraction (LEED) and density functional theory (DFT) analyses for the $(2\sqrt{3} \times 2\sqrt{3})$R30° structure. The height difference between the bright and dim molecules is consistent with real height differences between the molecules, and subtle differences in the molecular orientations of C_{60} on Au(111) and Ag(111) [29] have been replicated in the DFT calculations. We also have carried out STM experiments to study the dynamics of the bright-dim flipping observed near room temperature in this phase. The dynamical behavior observed at the C_{60}-Au(111) interface indicates that the C_{60} molecules induce many highly mobile vacancies in the top substrate layers, effectively amounting to interfacial melting well below the melting temperature of Au. This is likely the result of the weakening of the metal bonds in the surface layers due to the favorable C_{60}-metal interaction. Although the substrate layer beneath the C_{60} molecules is highly mobile, the C_{60} molecules themselves are stable and do not diffuse. The rapid diffusion of vacancies on a metal surface has been inferred from other studies, and in some cases adsorbates are observed to diffuse in concert with the vacancies [30,31]. Here we provide evidence for rapid diffusion beneath a stationary monolayer. We propose that a consequence will be a marked change of the frictional coupling between the C_{60} monolayer and the surface over a narrow temperature range near room temperature.

II. METHODS AND RESULTS

A. Low-temperature STM measurements

The low-temperature STM experiments were performed at Kiel using a homemade STM operated at 5.7 K in ultrahigh vacuum. The Au(111) sample and the etched W tips were prepared by Ar^+ bombardment and annealing. C_{60} was deposited from a tantalum crucible at a rate of ~1 ML/min as monitored by a quartz-crystal microbalance. During deposition, a residual gas pressure in the 10^{-8} mbar range was maintained and the sample was kept at room temperature. The results presented here correspond to approximately 20% of a completed C_{60} monolayer. All images were recorded in a constant-current mode.

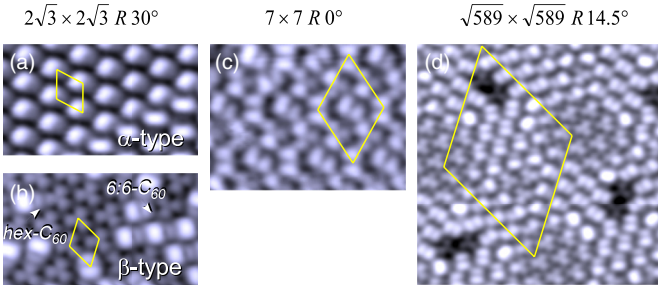

FIG. 1. (Color online) STM images recorded at sample voltages between 2 and 2.2 V of C_{60} islands on Au(111). (a),(b) 6.3 × 3.6 nm^2 images of two different domains of a $(2\sqrt{3} \times 2\sqrt{3})$R30° superlattice. (c) 6.3 × 4.7 nm^2 image of the (7 × 7)R0° structure. (d) 11.2 × 11.2 nm^2 image of a ($\sqrt{589}$x$\sqrt{589}$)R14.5° structure. Yellow rhombuses indicate the unit cells of the superstructures.

STM images recorded at a sample voltage Vs ≈ 2 V exhibit intramolecular structure (Fig. 1). These images reveal the bright contrast of the pentagons of the molecule, thus allowing the orientation of each C_{60} molecule to be determined [17]. The distributions of molecules under different conditions have been studied before [15], and, in the present study, we focus on the molecules which have the hex and 6:6 C-C orientations. These molecules are labeled in Fig. 1(b). The small asymmetry between the two lobes of the 6:6 C-C bond in the image suggests that the molecule is slightly tilted towards one of the carbon atoms of the bond.

Within the $(2\sqrt{3} \times 2\sqrt{3})$R30° structure, two distinct types of domains are observed, which are labeled α and β in Figs. 1(a) and 1(b). In the α domains, all molecules exhibit the same orientation as may be expected for molecules adsorbed to equivalent sites of the Au(111) substrate lattice. The β domains [Fig. 9(b) in [18]], however, contain two different molecular orientations that are imaged as bright and dim. Figures 1(c) and 1(d) display, respectively, STM images of the (7 × 7)R0° and the $\sqrt{589}$x$\sqrt{589}$R14.5°.

To gain further experimental insight into their geometries, we used a large-scale STM image [Fig. 2(a)] of the different superstructures. For clarity, the contrast of the image has been artificially enhanced by adding the topograph to its Laplace filtered copy. Using this image, C_{60} superstructures from different Au(111) terraces, which are separated by several steps, may be directly compared. Figures 2(b) and 2(c) are untreated subimages of Fig. 2(a) and, respectively, show ($\sqrt{589}$x$\sqrt{589}$)R14.5° and $(2\sqrt{3} \times 2\sqrt{3})$R30° β-type superstructures. The different apparent heights of the C_{60} molecules in these images are shown more quantitatively by cross-sectional profiles [Fig. 2(d)], which were measured along the indicated directions. In the ($\sqrt{589}$x$\sqrt{589}$)R14.5° superstructure, the 6:6 C-C appears 0.4 Å higher than the hexagon down [Fig. 2(d), blue line]. According to previous publications, both molecules are adsorbed on an unreconstructed Au(111) surface [17]. Therefore, this height difference is essentially due to different orientations of the C_{60} orbitals. Figure 2(b) also shows darker molecules that expose a hexagon to the STM tip, i.e., hex molecules. It has been suggested that these molecules are adsorbed on vacancies of the Au(111) substrate [17]. In the corresponding profile [Fig. 2(d), red

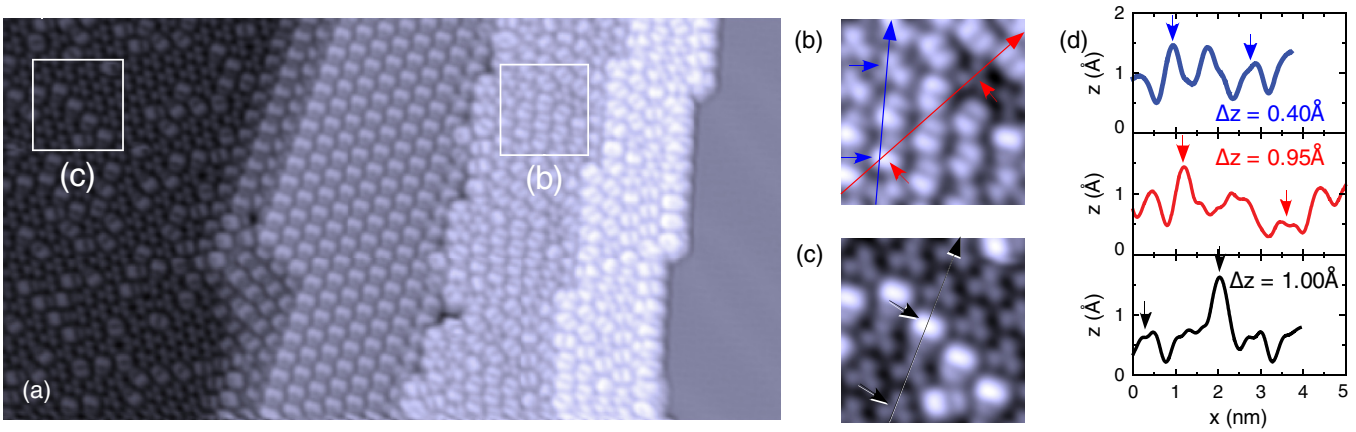

FIG. 2. (Color online) Constant-current images recorded at Vs = 2 V. (a) 34 × 17 nm^2 overview. (b),(c) 3.7 × 3.7 nm^2 subimages of (a) from the areas indicated by white squares showing ($\sqrt{589}$x$\sqrt{589}$)R14.5° and ($2\sqrt{3} \times 2\sqrt{3}$)R30° β-type superstructures. (d) Cross-sectional profile of (b) and (c) measured along the indicated lines. Short arrows highlight the molecules that were used to determine height differences.

line], these molecules appear 0.95 Å lower than the 6:6 C-C molecule. The height difference between hex molecules adsorbed on a vacancy and on the unreconstructed surface is therefore of 0.55 Å. On the ($2\sqrt{3} \times 2\sqrt{3}$)R30° β-type area, we measure a height difference of 1 Å between the 6:6 C-C bond down and hexagon-down molecules [Fig. 2(d), black line]. Taking into account the 0.4 Å height change resulting from the different orientations, the remaining 0.6 Å difference is consistent with a model where hex molecules of the ($2\sqrt{3} \times 2\sqrt{3}$)R30° β-type clusters are adsorbed at Au(111) vacancies and the 6:6 C-C molecules are adsorbed on top of the surface.

B. LEED measurements and analysis

The experimental procedures followed in this LEED study are similar to those described in an earlier paper for Ag(111)-($2\sqrt{3} \times 2\sqrt{3}$)R30°-$C_{60}$ [32], except that these experiments were carried out on a LEED instrument that has a channel plate image intensifier, and therefore the LEED patterns are projected onto a flat plane. Since the LEED intensity analysis is mostly sensitive to the locations of the peaks in the intensity-energy curves, this distortion has a negligible effect on the intensity analysis. The Au(111)-($2\sqrt{3} \times 2\sqrt{3}$)R30°-$C_{60}$ structure was prepared by dosing the C_{60} with the crystal at 370 °C and then annealing to 390 °C, which was just below the temperature where the monolayer C_{60} starts to desorb from the surface, and then slowly cooling the sample to 80 K. The LEED patterns observed after this procedure (Fig. 3) did not show evidence of any structures other than the ($2\sqrt{3} \times 2\sqrt{3}$)R30° structure.

LEED patterns were acquired for the energy range 40–450 eV, and intensities for 18 nonequivalent beams were extracted, for a total energy range of 5200 eV. The LEED calculations used the same theoretical methods as similar previous studies [29,32], using a scattering potential calculated from a superposition of atomic orbitals for the actual adsorption geometry [33]. This resulted in 12 sets of scattering phase shifts for symmetry-inequivalent C atoms and 2 sets for Au atoms (one for the top layer, another for the deeper layers).

The geometries included in the initial tests were top, hcp, fcc, bridge, and vacancy sites, and molecular orientations of hexagon down, pentagon down, and 6:6 C-C bond down. In light of results for C_{60} on other surfaces such as Ag(100) and Au(110) where C_{60} induces multiatom vacancies in the surface [34,35], we tested various vacancy configurations, including vacancies of 7, 13, 16, 19, and 20 atoms (with missing atoms in 1, 2, 2, 3, 4 Au layers, respectively), but those produced

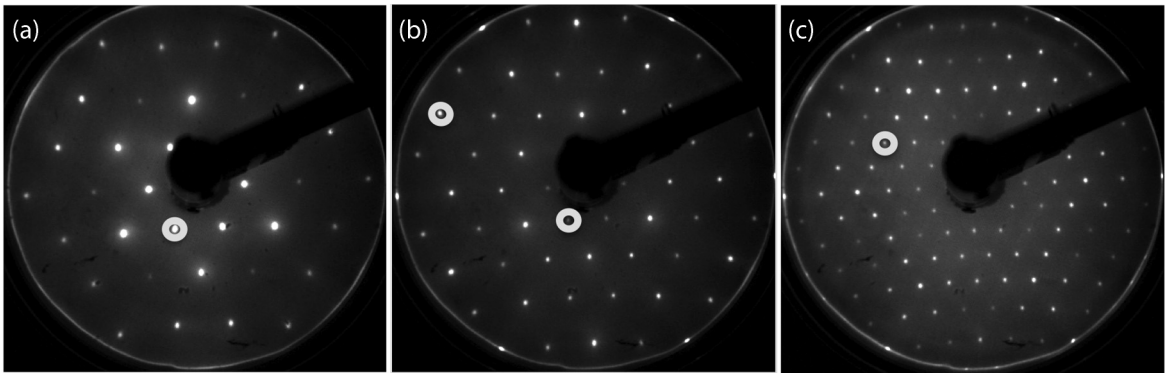

FIG. 3. LEED patterns from the Au(111)-($2\sqrt{3} \times 2\sqrt{3}$)R30°-$C_{60}$ structure at 80 K for electron energies of (a) 82, (b) 119, and (c) 275 eV. Representative first-order spots from the substrate and the C_{60} structure are indicated by gray annuli. These patterns are imaged on a flat plane and therefore the patterns appear distorted relative to a perfect hexagonal symmetry.

TABLE I. (Color online) Pendry R factors for the initial configurations of C_{60} on Au(111), and after optimization. The hex-par orientation was optimized to an 80:20 mixture of 0°:180° mirror-plane orientations. The figures show the hex and 6:6 C-C orientations and their mirror planes. The 10-atom vacancy model has seven missing atoms in the top layer and three in the next. Additional vacancy structures with 13, 16, 19, or 20 missing atoms in up to four substrate layers gave higher R factors.

					Vacancy		
Hex-par	Top	Hcp	Fcc	Bridge	1-atom	7-atom	10-atom
Initial run	0.68	0.81	0.83	0.82	0.66	0.84	0.86
Optimized	0.40				0.39		

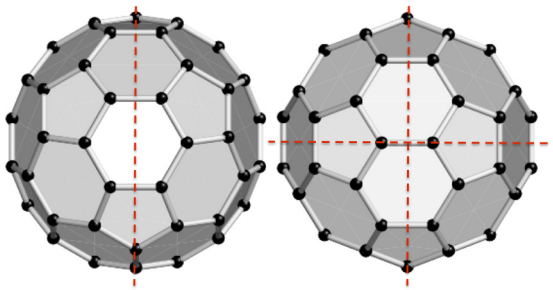

considerably worse agreement than a single-atom vacancy. Domain averaging was used to achieve the symmetry of the LEED pattern of threefold rotation plus a mirror plane. The only C_{60} orientation that gave R factors below 0.90 at this stage of the calculation was the hexagon down, with the C_{60} mirror plane parallel to the substrate mirror plane (hex-par). These results for this C_{60} orientation in different sites before optimization are given in Table I. With these results, we were able to rule out all sites aside from the top and vacancy sites, although we could not distinguish between them. These were further refined, with the final R factors given in Table I. There is a subtle difference in the 0° and 180° orientations of the C_{60} mirror plane on the top or vacancy site on fcc(111). Although we found no preference in orientation for the hex-vac structure of C_{60} on Ag(111), we found a clear preference for the 0° orientation on Au(111), which corresponds to the noncentral pentagon (hexagon) along the mirror plane being located over an Au atom in the second (third) substrate layer. Mixtures of hex-par molecules in top and vacancy sites were also tested, but produced higher R factors.

In light of the STM studies, which indicate mixtures of C_{60} orientations even at low temperature, we carried out the analysis for mixtures in the same way as presented earlier for C_{60}/Ag(111) [29]. The results of this analysis are shown in Table II. The best R factor is 0.33. This is not as low as the corresponding R factor for the case of C_{60} on Ag(111), which was 0.24. Therefore, we also considered the possibility that the Au(111) reconstruction is not entirely lifted and there may be some regions of hcp stacking in the top layers, as observed for benzene on Au(111) [36]. However, including a fraction of hcp stacking in the analysis resulted in worse agreement.

In these calculations, the 6:6 C-C bond orientation was tested in both the parallel and 30° orientations, relative to the substrate mirror plane. The LEED intensities are mostly insensitive to the difference in these orientations. In light of the STM observations, which suggest a tilt of this bond, we have also tested C_{60} molecules tilted up to 15° from flat. For an undistorted molecule, the best agreement is found for a 10° tilt. However, when the molecule is allowed to relax, the best agreement is for an untilted molecule, but with a distortion that produces a 10° tilt in the 6:6 C-C bond. The best R factors were found for 80:20 mixtures of hex and 6:6 orientations, which is consistent with the STM observations for the highest annealing temperatures [15].

TABLE II. Pendry R factors for the mixtures of orientations of C_{60} on Au(111). The hex-par configurations have an 80:20 mixture of 0°:180° mirror-plane orientations. The result that is most consistent with all techniques is indicated in bold type.

	Hex-par top	Hex-par vac	6:6 C-C top 0°/30°	6:6 C-C vac 0°/30°
Hex-par top	0.40		0.38/0.37	0.37/0.36
Hex-par vac		0.39	**0.34**/0.33	0.34/0.34
6:6 C-C top			0.64/0.60	
6:6 C-C vac				0.64/0.58

Although the LEED analysis is rather ambiguous for differentiating between the top and vac site and between 0° and 30° orientation of the C-C molecules, it does rule out all other sites, orientations, and mixtures. The hex-top can be ruled out by earlier DFT results [32], and the 30° orientation of the 6:6 C-C bond molecule can be ruled out by the STM results [18]. This leaves two site possibilities for the 6:6 C-C bond molecule, namely, top and vacancy. The results of the configuration mixing are given in Table III, indicating that in each case, the best mixture has about 80% hex-par vac. This low amount of the C-C molecules on the surface may account for the insensitivity of the LEED to the details of the structure. Therefore, the C-C structures were optimized without allowing relaxations in the C_{60} molecule or the substrate. The best-fit structural parameters for the hex-par vac, and the two 6:6 C-C configurations are given in Table IV. Both sites for the 6:6 C-C molecules are included in this table since the LEED cannot distinguish between them. However, the top site geometry is more compatible with the STM and DFT results (see discussion). Representative LEED spectra for the most

TABLE III. Pendry R factors for the different mixing ratios for the hex-par vac mixed with either 6:6 C-C top 0° or 6:6 C-C vac 0° structures. A mixing ratio of 100:0 refers to 100% hex-par vac molecules.

Mixing	6:6 top	6:6 vac
100:0	0.39	0.39
90:10	**0.34**	**0.34**
80:20	**0.34**	**0.34**
70:30	**0.36**	**0.35**
60:40	0.39	0.38
50:50	0.42	0.41
40:60	0.45	0.45
30:70	0.60	0.59
20:80	0.65	0.64
10:90	0.71	0.70
0:100	0.89	0.87

TABLE IV. (Color online) Best-fit parameters for C_{60} on Au(111) according to the LEED analysis. Both sites for the 6:6 C-C molecule are shown, since the LEED analysis does not distinguish between them. dz(C_{60}) refers to the vertical distance between the center of mass of the C_{60} molecule and the center of mass of the top substrate layer. The d(Au-C) value corresponds to the shortest bond distance between C and Au atoms. The other dz values are the vertical interlayer spacings, measured from the center of mass of the layers. Δ corresponds to the average intralayer buckling amplitude (not included for the 6:6 structures). The bulk interlayer spacing of Au(111) is 2.35 Å. The definition of the parameters is given in the drawing below.

Parameter	Hex-par vac (Å)	6:6 C-C top (Å)	6:6 C-C vac (Å)
d(Au-C)	2.4 ± 0.1	2.3 ± 0.2	2.8 ± 0.2
dz(C_{60})	5.1 ± 0.1	5.7 ± 0.2	5.1 ± 0.2
dz(Au_1-C)	1.8 ± 0.1	2.2 ± 0.2	1.6 ± 0.2
dz(Au_1-Au_2)	2.33 ± 0.03	2.32	2.32
dz(Au_2-Au_3)	2.36 ± 0.4	2.35	2.35
dz(Au_3-Au_4)	2.30 ± 0.06	2.35	2.35
Δ_1	0.05 ± 0.04		
Δ_2	0.02 ± 0.04		
Δ_3	0.01 ± 0.05		

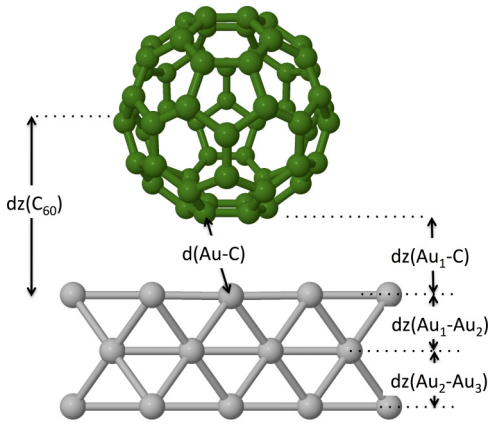

favorable mixture of hex-par vac and 6:6-0° top are shown in Fig. 4.

C. DFT studies for mixed configurations of C_{60} on Au(111) and Ag(111)

In order to explore this further, we have carried out DFT calculations for mixed configurations of C_{60} on Au(111). We also looked at C_{60} on Ag(111), since the LEED analysis was unambiguous in that case. Even though thermodynamically the C_{60} molecules prefer to sit on a vacancy site on the Ag(111) and Au(111) surfaces [32], the activation energy for vacancy formation can be high, making the ground state not easily accessible. The LEED and STM results presented earlier are consistent with a mixture of different configurations of molecules, and therefore we have extended the DFT studies to a larger unit cell to investigate mixed phases.

The setup for the DFT calculation is shown in Fig. 5 and the computational procedures were presented earlier [12,29]. In these calculations, we used a $(4\sqrt{3} \times 2\sqrt{3})$R30° surface supercell to accommodate two C_{60} molecules. The left C_{60} sits on a vacancy site with one of the hexagons facing down the

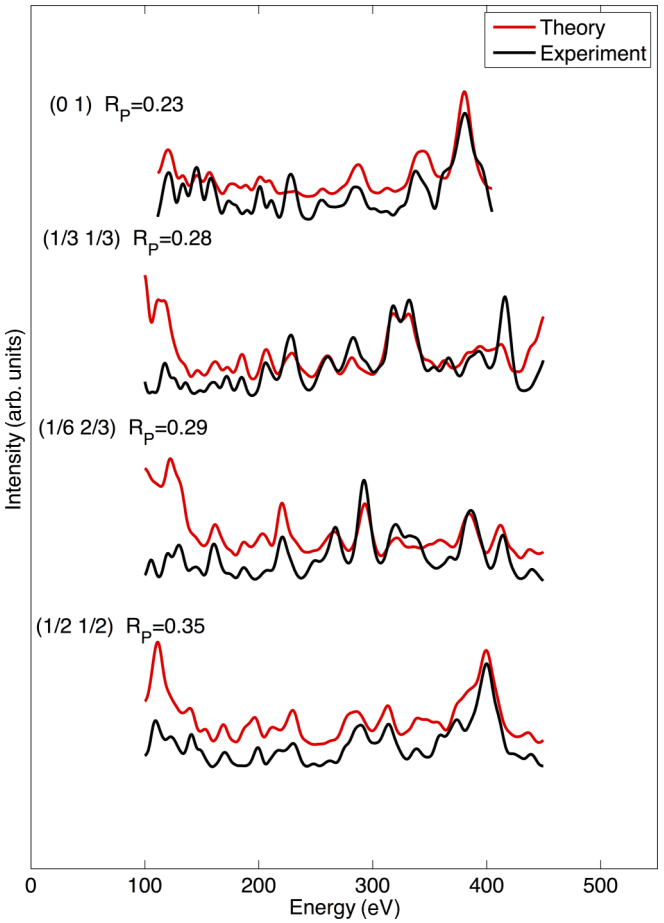

FIG. 4. (Color online) Representative LEED spectra from the best-fit mixture of 80% hex-par vac and 20% 6:6 C-C top for C_{60} on Au(111). The full data set is provided in Ref [37].

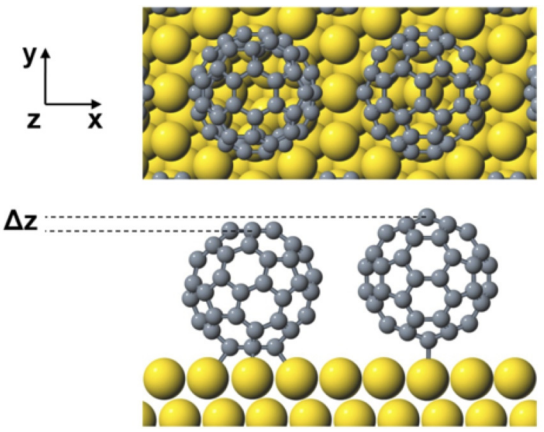

FIG. 5. (Color online) $(4\sqrt{3} \times 2\sqrt{3})$R30° surface supercell used in the DFT calculation for mixed configurations of C_{60} on Ag(111) and Au(111). Top (bottom) panel is for top (side) view. The left (right) C_{60} sits on a vacancy (top) site with a hexagon (short C-C bond) facing down to the surface. Δz labels the height difference between the two C_{60} molecules on different sites. This is the starting/reference orientation of the system for the energy-orientation plot in Fig. 6. The orientation change of the right C_{60} involves the anticlockwise rotation along the z axis, and three tilt angles for each rotation.

TABLE V. Calculated vacancy formation energy (E_{vac}) and adsorption energies in eV per C_{60} for the indicated configurations of C_{60} on Ag(111) and Au(111). A range of values reflects the extra Ag atoms being located on the surface between molecules (low number) or in a bulk site (high number).

Configuration	Ag(111)	Au(111)
E_{vac}	0.76	0.83
Hex-hcp	1.45	1.23
Hex-top	1.20	0.84
6:6-top	1.27	0.99
Hex-vac	1.44–1.74	1.26–1.76
6:6-vac	0.94–1.24	0.55–1.05
Hex-vac + hex-top	1.36–1.51	1.06–1.31
Hex-vac + 6:6-top	**1.40–1.55**	**1.17–1.42**
Hex-vac + 6:6-vac	1.22–1.52	0.93–1.43

surface and its mirror plane is parallel to the mirror plane of the substrate, which was found previously to be the most stable configuration [32]. To maintain the 10 Å distance between C_{60} molecules, the right C_{60} sits over a substrate atom site. We have tried different adsorption configurations of this C_{60} molecule, including the hex and 6:6 C-C orientations discussed earlier. To find the preferred orientations, we varied the orientation of the right C_{60} by rotating it around both the z axis (perpendicular to the surface) and the x axis to give it a tilt angle (see Fig. 5). In each calculation, the bottom two metal atomic layers are fixed at their bulk positions, and the remaining top three metal layers and the C_{60} molecules are allowed to fully relax to the local minimum, for each tilt angle and azimuthal orientation.

In analogy with our earlier calculations for a the similar structure on Ag(111) [29], we used a $(6 \times 6 \times 1)$ k-point mesh for one C_{60} molecule and a $(3 \times 6 \times 1)$ k-point mesh for two C_{60} molecules to reach an error below 0.01 eV for adsorption energies. We report in Table V our calculated minimum energies for C_{60} on both Ag(111) and Au(111) using the same k-point meshes. Note that for a single C_{60} orientation, the hex-vac is the most stable (has the highest adsorption energy), but for a mixed phase, the hex-vac +6:6-top is the most favorable.

Figure 6 shows the change in adsorption energy per C_{60} vs tilt angle for rotations around the z axis at 0, 30, 60, 90, 120, and 150 degrees when the right C_{60} sits with a 6:6 C-C bond on a top site. The configurations can be divided into two groups. One group has 0, 60, and 120 degrees rotation around the z axis, where the 6:6 C-C bond points to the nearest-neighbor substrate atom; the other has 30, 90, and 150 degrees, where the 6:6 C-C bond points to the next-nearest-neighbor substrate atom or along the mirror plane of the substrate. On Ag(111) [Fig. 6(a)], the tilt angle for the 0° group decreases to 4.6° after relaxation (the initial tilt angle is at 10°), while for the 30° group, the tilt angle increases slightly to 11.5° after relaxation. The energy variation is asymmetric vs the tilt angle at different rotations around the z axis. The energy variation vs the tilt angle is much smaller for the 0° group than the 30° group. The 0° and 120° orientations have the lowest energy, i.e., 0.05 eV lower than the configuration of hex-vac + hex-top (the horizontal dotted line). For the 30° group, they are close to the lowest energy of the 0° group only at large tilt angles. In contrast, on Au(111) [Fig. 6(b)], the 30° group almost always has lower energy than the 0° group, with the most stable one being 0.12 eV lower than the hex-vac + hex-top. Although there is still less variation in the energy vs tilt angle for the 0° group, the tilt angle is at 11.5° for this group, the same as the 30° group and larger than the 0° group on Ag(111). The 30° group on Au(111) also has less energy variation than on Ag(111). Overall, the energy for the 6:6 C-C orientation of the C_{60} on the top site sitting next to the hex-vac is lower than for the hex-top orientation on both Ag(111) and Au(111). More importantly, the preferred in-plane orientations of the 6:6 C-C differ by 30° and are consistent with the present and earlier STM results [5,17].

Because the left C_{60} sits on a vacancy site, there is a height difference between the tops of the two C_{60} molecules, which is $\Delta z = 0.5$ Å and 0.7 Å on Ag(111) and Au(111), respectively. This height difference will appear in STM as an overall dim-bright contrast. Figure 7 shows the simulated STM images on the two surfaces. On Ag(111), the preferred orientation is 0° or 120° with a small tilt angle of 4.6°, while on Au(111), it is 30° or 90° with a tilt angle of 0°, although a large tilt angle of 11.5° gives an almost degenerate energy. By sampling the lowest occupied molecule orbitals (LUMO) at +1 V bias, the contrast of different tilt angles on two surfaces agrees well with previous high-resolution STM [5,18]. The preferred orientations of bright C_{60} also agree with experiment, where there is a 30° difference for the two substrates.

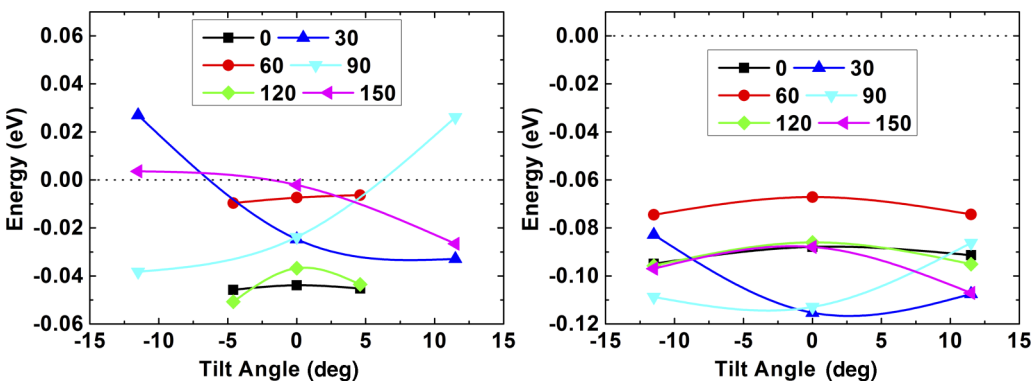

FIG. 6. (Color online) Adsorption energy per C_{60} vs tilt angle of the right C_{60} at different rotational angles (see Fig. 5) on (a) Ag(111) and (b) Au(111). The energy scale is relative to the hex-vac + hex-top configuration (dotted horizontal line).

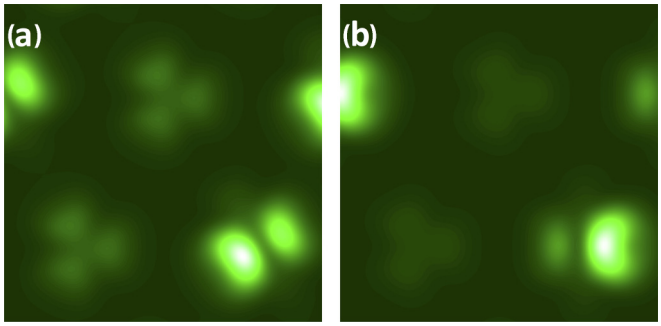

FIG. 7. (Color online) Simulated STM image of the mixed configurations at +1 V for the right C_{60} (a) at 120° with tilt angle of 4.6° on Ag(111) and (b) at 90° on Au(111) with tilt angle of −11.5° (see Fig. 5).

D. STM studies of the dynamics of the C_{60} molecules on Au(111)

Earlier studies of C_{60} on Au(111) have observed that the molecules "flip" between the bright and dim states at room temperature, and they have measured the flipping rate to be 1.0×10^{-4} s^{-1} for both bright to dim and dim to bright [15]. (That study found a higher flipping rate in an incommensurate phase, which was not part of this study.) Such flipping in the $(2\sqrt{3} \times 2\sqrt{3})$R30° phase has also been studied on Ag(111), where it was found to be temperature dependent and it was determined that there is an energy barrier for flipping (each way) of 0.84 eV [29]. We have carried out similar measurements for the case of C_{60} on Au(111).

The Au(111) surface was prepared by sputtering (Ar^+, 0.5–2.0 keV, 15 min) and annealing cycles (700 K, 15–30 min). The Au(111)-$(2\sqrt{3} \times 2\sqrt{3})$R30°-$C_{60}$ structure was obtained by dosing the C_{60} (3.6 ML min^{-1}) with the crystal at 670 K and the dynamics of the bright-dim C_{60} flipping was studied using an Omicron variable-temperature STM in the temperature range from 250 to 320 K. The bright-dim ratio was determined for different temperatures by manually counting individual molecules on the STM images and averaging over a large population (several hundreds) to achieve good statistics. Several STM movies were also recorded at different temperatures in the range of 250 to 320 K by recording several tens of drift-corrected STM images of the same area. The flips between the bright and dim molecular states were counted by subtracting consecutive images. Meaningful flipping rates could only be obtained in the range from 257 to 293 K. Below 257 K, the flipping rate is too low and the scan time is too long to get accurate measurements. Above 300 K, the flipping rate depends on the scanning parameters (scanning size and speed), indicating that molecules start to flip more than one time between the two states during the scan, even under the fastest scanning conditions (30 s per image). These points were therefore disregarded for the analysis.

Figures 8(a) and 8(b) show STM images taken at 272 and 298 K, respectively. All molecules are either in the bright or dim state. The insets show difference images between two successive frames. Here a bright spot indicates that a molecule has flipped from dim to bright and a dark spot indicates a flip from bright to dim, while other molecules with intermediate contrast stay in the same state. The flipping rate drastically increases with the temperature. These difference images show that two opposite flips (bright to dim and dim to bright) are often correlated (paired), i.e., appear next to each other. Such correlation had already been observed in the study on Ag(111) [29]. However, some of the flips do not have an obvious correlation with a neighboring flip. Figure 8(c) identifies examples of these flips and Fig. 8(d) shows the temperature dependence of the fraction of flips involving nearest-neighbor molecules (NN), next-nearest neighbors (NNN), and uncorrelated flips on the Au(111) substrate. It turns out that NNN flips are rare and are therefore are likely to be uncorrelated. Clearly, the fraction of NN flips decreases at the expense of uncorrelated flips with increasing T. Also, the bright to dim flipping rate is essentially equal to the dim to bright flipping rate (not shown), indicating an equilibrium situation.

The logarithms of the flipping rates for correlated and uncorrelated flips are plotted in Fig. 8(e) as a function of the inverse of T. The flipping rates are identical, to within the error, for bright to dim and dim to bright, and the values on the graph are for one of these. Assuming an Arrhenius behavior, we deduce a flip activation energy of 0.73 ± 0.03 for all flips. If we separate the NN flips from the uncorrelated flips, we deduce 0.66 ± 0.03 eV for correlated flips and 0.93 ± 0.03 eV for uncorrelated flips. The temperature dependence of the bright to dim ratio appears to be very weak; the percentage of bright molecules stays in the range of 0.40 ± 0.03 in the temperature range of 257 to 310 K. The variations are of the order of the error bar for a single temperature. We have also compared the fraction of NN correlated flips on both Au(111) and Ag(111) substrates. On Ag(111), the fraction of NN correlated flips remains constant at about 77% over the temperature range studied, whereas on Au(111), it decreases from about 86% to 52%.

To gain some insight on the differences in the dynamics of C_{60} on Au and Ag substrates, additional *ab initio* calculations were performed to compare the activation energy for the diffusion of a vacancy in both systems, as C_{60} flipping involves vacancy diffusion [29]. For this, we used the Vienna *ab initio* Simulation Package (VASP) based on the DFT using the projector-augmented wave (PAW) method. The electronic exchange and correlation contribution is described using the generalized gradient approximation, GGA-PBE. The parameters linked to the numerical implementation of the DFT, e.g., the plane-wave cutoff E_{cut} and the density of k points sampling the Brillouin zone, were converged by means of a series of test calculations on bulk gold and silver. The chosen values for E_{cut} (450 eV) and the size of the Monkhorst-Pack k-points mesh ($16 \times 16 \times 16$) achieve a precision for the bulk total energy smaller than 1 meV. For the calculations using slabs, we used a similar k-grid mesh.

The surfaces were modeled using asymmetric slabs made of eight layers (four fixed and four free layers) and a vacuum thickness of about 12 Å. The C_{60} layer is not taken into account in these calculations. The theoretical lattice parameters are 4.16 and 4.15 Å for Au and Ag, respectively, compared to the experimental values of 4.08 and 4.09 Å, respectively. Surface vacancy formation energies were calculated for systems containing either 4, 9, or 16 atoms per layer and it was found that a system with 9 atoms per layer gives accurate values within 20 meV for Ag and 40 meV for Au. The herringbone reconstruction of the Au(111) surface was not considered in the

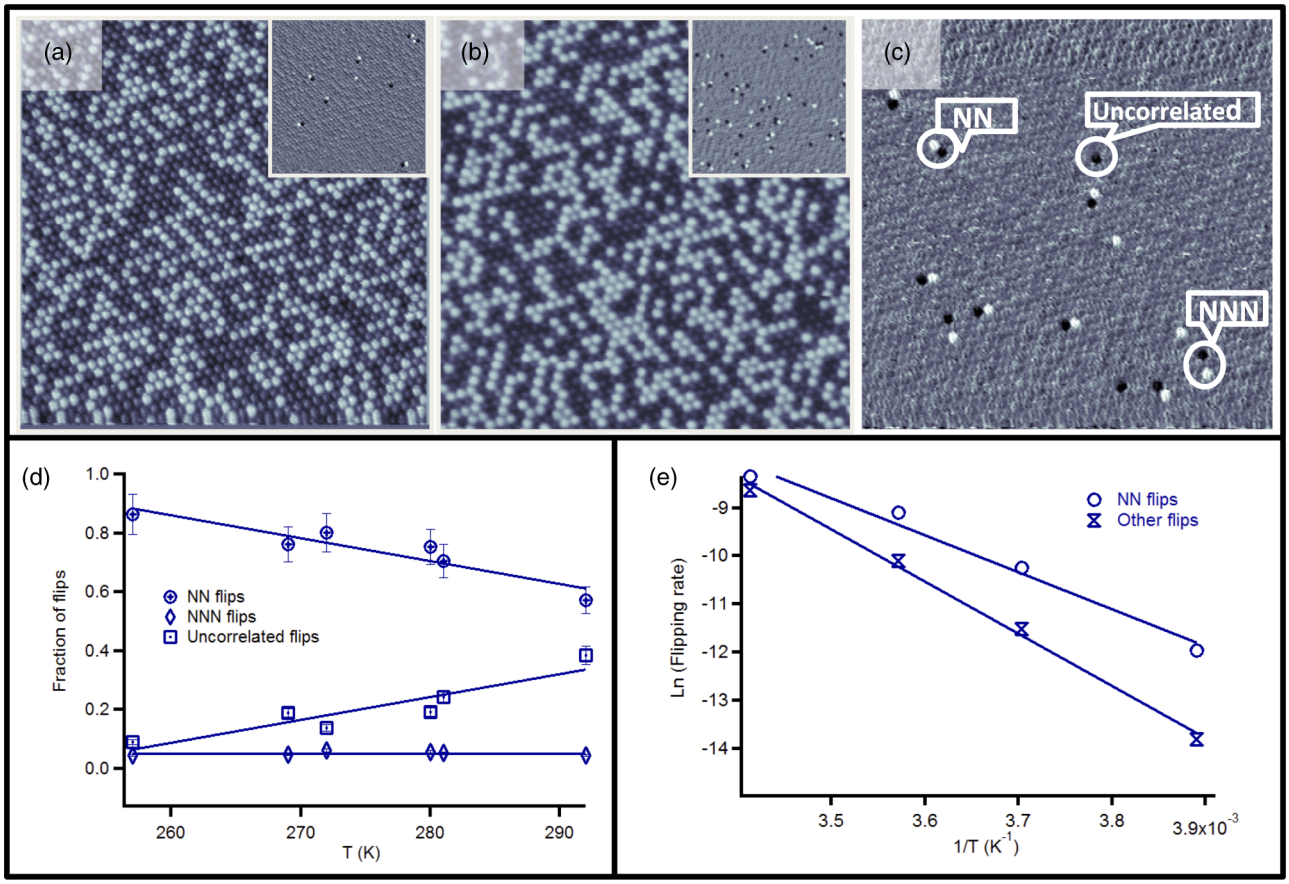

FIG. 8. (Color online) (a) 40 × 40 nm^2 STM image of Au(111)- $(2\sqrt{3} \times 2\sqrt{3})$R30°-$C_{60}$ at T = 272 K and tunneling parameters I = 0.09 nA, V = +2.2 V. Inset: Difference between the image shown and the previous one, 69 s earlier. (b) 40 × 40 nm^2 STM image of same surface at T = 298 K and I = 0.06 nA, V = +2.3 V. The inset showing the difference of two successive frames indicates a higher rapid flipping rate at higher temperature. (c) Difference between two successive STM images (40 × 40 nm^2) of Au(111)- $(2\sqrt{3} \times 2\sqrt{3})$R30°-$C_{60}$ at T = 280 K recorded 81 s apart. Examples of NN, NNN, and uncorrelated flips are outlined. (d) Temperature dependence of the fraction of NN, NNN, and uncorrelated flips on Au(111)- $(2\sqrt{3} \times 2\sqrt{3})$R30°-$C_{60}$. (e) Plot of the natural logarithm of the bright to dim or dim to bright flipping rate (events/nm^2 s) as a function of inverse temperature for NN flips and other flips. The slopes of the graph indicate activation energies of 0.66 ± 0.03 eV and 0.93 ± 0.03 eV, respectively.

present calculations [the $(2\sqrt{3} \times 2\sqrt{3})$R30°-$C_{60}$ phase lifts the reconstruction]. The calculated vacancy formation energies are 0.63 and 0.57 eV for Au and Ag, respectively. The difference between these values and those given in Table V is mainly due to the different exchange-correlation functionals used. The results reported in Table V used local-density approximation (LDA), whereas the ones here used Perdew-Burke-Ernzerhof (PBE). Because LDA generally overbinds and PBE underbinds for metals, the two sets of values for the vacancy formation energies in this paper can be considered to be upper and lower bounds. More important for the results reported here, however, is that the energy differences between the vacancy formation energy of Ag and Au(111) are essentially the same for both functionals, and energy comparisons for each method are internally consistent. Table VI shows the calculated activation energies (using PBE) for vacancy diffusion on Ag and Au(111), for different movements of the vacancy.

All of these values are close to each other and are about the same for both metals, indicating that the difference between the flip activation energies does not originate from the vacancy diffusion itself, but might be due to different interactions between the C_{60} and metal substrates. We note that the activation energy is smaller for surface diffusion than for bulk diffusion, on both substrates, and that the calculated activation energies are smaller than the experimentally derived flip activation energies. As reported earlier (Table V), there is a difference between the adsorption energies on Au(111) and Ag(111), indicating a generally higher molecule-surface interaction for Ag. This is consistent with the lower activation energy found for the C_{60} on the Au substrate. The results in Table VI may provide some insight into why surface to bulk diffusion is more likely relative to surface to surface

TABLE VI. Calculated activation energies for vacancy diffusion in Au and Ag.

Activation energy (eV)	Au	Ag
Surf → surf	0.51	0.51
Bulk → bulk	0.58	0.54
Surf → bulk	0.31	0.47
Bulk → surf	0.62	0.40

diffusion on the Au substrate compared to Ag, in agreement with the experiments. We want to make it clear, however, that these calculations are for the clean surfaces, and not the adsorption systems—clearly the presence of C_{60} will make a big difference to the energetics of the diffusion processes.

III. DISCUSSION

The STM results for C_{60} adsorption on Au(111) indicate that the most stable monolayer phase of the C_{60} at the temperatures studied is the commensurate $(2\sqrt{3} \times 2\sqrt{3})$R30° structure, which has a disordered mixture of hex and 6:6 C-C C_{60} orientations. In this phase, the molecules are observed to flip between the two molecular orientations at temperatures near room temperature (RT). The LEED, STM, and DFT results indicate that the hex molecules reside in vacancies, a structure that requires either elevated temperatures (above RT) or considerable time to form because of the energy required to form the vacancy. Although the DFT indicates that the hex-vac configuration is the ground state of the C_{60} molecules, a significant fraction of other molecules is present on the surface, identified in STM studies as having a 6:6 C-C bond facing the substrate. These molecules are imaged as being higher (and brighter) than the hex molecules. It was possible to determine that the difference in orientation itself results in an apparent height difference of 0.4 Å in the STM images, implying an actual height difference of 0.6 Å, which is nearly the same as the height difference determined by the LEED and DFT.

A comparison of the structural parameters found for C_{60} on Ag(111) [29] and Au(111) is given in Table VII. The height differences measured using the three techniques allows us to conclude that there is a concurrence and consistency of the three techniques concerning the adsorption sites of the two molecular orientations. The presence of the vacancy allows the hex-vac C_{60} to sit significantly deeper in the surface than the 6:6 C-C molecule, and more deeply on Au(111) than on Ag(111), although the difference is nowhere near the interlayer spacing of 2.35 Å because the molecule is too large to penetrate very far into a single-atom vacancy.

Table VII also summarizes some of the main energy parameters that characterize the flipping between the bright and dim molecules, including the energy difference between the two states as deduced from the temperature dependence of the bright-dim ratio measured in the STM experiments. These values are considerably smaller than the values calculated in DFT at T = 0 K (Table V). If the values were as large as the calculated values, it would be much easier to measure in the experiment. Therefore, we believe that the discrepancy is mostly due to the lack of entropy effects in the modeling. Entropy is undoubtedly a significant factor in the experimental result; in fact, the entropy must provide the stabilization of the 6:6-top + hex-vac mixture. Both the molecular motion and the fact that the substrate atoms are highly mobile will have an impact on a comparison to the calculated static situations. The C_{60}-C_{60} interactions, which cannot be simulated accurately in a disordered system by a two-molecule unit cell, are most likely less of a factor in this discrepancy because comparisons of the calculated energies for the 1 C_{60} vs. 2 C_{60} supercells suggest very weak interactions between them.

TABLE VII. Height difference in Å between the tops of the bright (6:6-top) and dim (hex-vac) molecules on Ag(111) and Au(111). The height difference for the LEED results was obtained by adding 0.2 Å (the difference in radius of C_{60} for the two orientations) to the difference in their center of masses from Table IV.

	Ag(111)			Au(111)		
	Height difference between bright and dim					
	LEED	STM	DFT	LEED	STM	DFT
	0.5 Å	0.3 Å	0.5 Å	0.8 Å	0.6 Å	0.7 Å
Flipping parameters						
T **range**	280–330 K			255–295 K		
$E_{correlated}$				0.66 ± 0.03 eV		
$E_{uncorrelated}$				0.93 ± 0.03 eV		
$E_{average}$	0.84 ± 0.05 eV			0.73 ± 0.03 eV		
E_{bright}-E_{dim}	0.07 ± 0.02 eV			−0.02 ± 0.03 eV		

The difference of site and orientation for the bright and dim molecules implies that flipping from one to the other involves a concerted motion of a substrate atom and a molecular rotation. The lack of long- or short-range ordering of the bright-dim molecules in the $(2\sqrt{3} \times 2\sqrt{3})$R30° structures on both Au(111) and Ag(111) suggests that the C_{60}-C_{60} interactions do not drive this uncorrelated flipping motion, which increases its frequency with temperature and therefore appears to be primarily entropic. This is unlike the case of bulk C_{60} and also the surface of bulk C_{60}, where the molecular ordering into a four-sublattice structure at low temperature is driven by anisotropic C_{60}-C_{60} interactions that favor an arrangement where a C-C bond of one molecule points toward the pentagon of a neighboring C_{60} molecule [38,39].

In comparing the ratio of bright to dim obtained in the LEED results to the STM, we find that there is quite good agreement. The LEED experiments were both performed at sample temperatures well below any measureable flipping activity, therefore we compare the LEED results to the lowest-T equilibrium STM results. The fraction of bright molecules in the LEED analysis was 0.5 ± 0.1 for Ag and 0.2 ± 0.1 for Au. In the STM counts, the fractions were 0.6 and 0.4, respectively, both slightly higher than the LEED values. This difference might be due to some conversion from bright to dim as the temperature decreases. In addition, the LEED measurements average over a much larger region than measured with STM, which might lead to a difference in the values. The fraction of bright molecules from our STM study on Au at room temperature is the same as the earlier STM study [15], and the flipping rate that we measured was somewhat higher, about 4×10^{-4} s^{-1}, compared to 1.0×10^{-4} s^{-1} reported in the earlier study, but this could be accounted for by a difference in sample temperature or by counting statistics. In the earlier study on Ag, [29] we had used the earlier value for Au to compare the activation energies on the two surfaces, and arrived at a wrong conclusion because of this discrepancy. A comparison of the dynamics on the two different metals suggests that some of the vacancies diffuse below the surface layer on Au(111), which may be due to the fact that the surface atoms on clean Au(111) are already weakly bound, a fact exemplified by its surface reconstruction.

The flipping behavior on both Au(111) and Ag(111) near room temperature is consistent with the diffusion of highly mobile vacancies in the top layer (or layers) of the substrate, while the C_{60} monolayer remains stationary. Such motion amounts to a melted interfacial layer of metal. The rapid diffusion of vacancies on surfaces has been inferred in earlier studies, but on clean metal surfaces, vacancies are rare, whereas the vacancies observed here comprise up to 8% of the surface sites. Since surface melting is not observed on the clean surfaces, it must be induced by the C_{60}-substrate interaction, which reduces the metal-metal interaction through the hybridization of C_{60} orbitals. As a result, we expect that the frictional coupling of the C_{60} monolayer to the surface will be significantly reduced as a result of this melting.

The flipping between states that image at different brightness has also been studied for C_{60} on Ag(100) [40]. In that case, there are three different species, interpreted as molecules located on top of atoms (bright), in one-atom vacancies (medium), or five-atom vacancies (dark). That also was found to be an equilibrium situation at temperatures near room temperature and the observations were similar to those reported here, namely, that the flipping appears to be temporally random but spatially correlated for certain types of flips. Interestingly, in that case, the flips between dark and medium and between dark and bright, both of which involve the five-atom vacancies, are spatially correlated, whereas flips involving bright to medium, which would be expected to be more similar to the case we have presented here, are not. It was suggested that this might be a result of the relative high mobility of a single-atom vacancy compared to a five-atom vacancy, i.e., a five-atom vacancy moving in a concerted way is slower and less probable compared to a one-atom vacancy.

Finally, we note that a phenomenon observed for C_{60} on Ag(111) is absent from the monolayer observations for C_{60} on Au(111) [41], the so-called superbright molecules, which image as very bright using STM and comprise about 0.5% of the monolayer. The origin of such molecules is not yet clear, but one proposal was that the superbright molecules are pushed up by Ag adatoms [41]. Given the high mobility of Au surface atoms, and the propensity of C_{60} molecules to climb onto Au(111) islands [24], it seems plausible that such a mechanism could occur on Au(111), but we have not observed any such molecules in the equilibrium monolayer, nor have any been reported.

ACKNOWLEDGMENTS

We thank D. L. Allara for the use of the Au(111) crystal in LEED experiments and Kristin Marino for assistance with preparing figures. A.S. gratefully acknowledges DAAD for the financial support for summer research at Penn State. We also thank the CNRS for the INCAS project (No. PICS05892) funding, Academy of Finland Projects No. 130818 and No. 263634, and CSC-IT Center for Science. The work at the Ames Laboratory was supported by the US Department of Energy, Office of Science, Basic Energy Sciences, Materials Science and Engineering Division. Additional capabilities were made possible from LDRD funding for materials discovery and design. Ames Laboratory is operated for the US Department of Energy by Iowa State University under Contract No. DE-AC02-07CH11358.

[1] E. I. Altman and R. J. Colton, Surf. Sci. **279**, 49 (1992).
[2] E. I. Altman and R. J. Colton, Phys. Rev. B **48**, 18244 (1993).
[3] E. I. Altman and R. J. Colton, Surf. Sci. **295**, 13 (1993).
[4] E. I. Altman and R. J. Colton, J. Vac. Sci. Technol. B **12**, 1906 (1994).
[5] W. Chen, H. D. Zhang, H. Huang, L. Chen, and A. T. S. Wee, ACS Nano **2**, 693 (2008).
[6] C. C. Kuo, C. H. Lin, W. W. Pai, K. C. Lin, and T. B. Tang, Surf. Rev. Lett. **14**, 739 (2007).
[7] P. Rudolf, in *Fullerenes and Fullerene Structures*, edited by H. Kuzmany, J. Fink, M. Mehring, and S. Roth (World Scientific, Singapore, 1996), p. 263.
[8] T. Sakurai, X. D. Wang, T. Hashizume, V. Yurov, H. Shinohara, and H. W. Pickering, Appl. Surf. Sci. **87-88**, 405 (1995).
[9] T. Sakurai, X. D. Wang, Q. K. Xue, Y. Hasegawa, T. Hashizume, and H. Shinohara, Prog. Surf. Sci. **51**, 263 (1996).
[10] A. Tamai, A. P. Seitsonen, R. Fasel, Z. X. Shen, J. Osterwalder, and T. Greber, Phys. Rev. B **72**, 085421 (2005).
[11] L. H. Tjeng, R. Hesper, A. C. L. Heessels, A. Heeres, H. T. Jonkman, and G. A. Sawatsky, Solid State Commun. **103**, 31 (1997).
[12] L. L. Wang and H. P. Cheng, Phys. Rev. B **69**, 165417 (2004).
[13] X.-D. Wang, S. Yamazaki, J.-L. Li, T. Hashizume, H. Shinohara, and T. Sakurai, Scanning Microsc. **8**, 987 (1994).
[14] J. Wen and J. Ma, Langmuir **26**, 5595 (2010).
[15] J. A. Gardener, G. A. D. Briggs, and M. R. Castell, Phys. Rev. B **80**, 235434 (2009).
[16] C. Rogero, J. I. Pascual, J. Gomez-Herrero, and A. M. Baro, J. Chem. Phys. **116**, 832 (2002).
[17] G. Schull and R. Berndt, Phys. Rev. Lett. **99**, 226105 (2007).
[18] G. Schull, N. Néel, M. Becker, J. Kröger, and R. Berndt, New J. Phys. **10**, 065012 (2008).
[19] L. Tang, X. Zhang, and Q. Guo, Surf. Sci. **604**, 1310 (2010).
[20] L. Tang, X. Zhang, Q. Guo, Y. N. Wu, L. L. Wang, and H. P. Cheng, Phys. Rev. B **82**, 125414 (2010).
[21] L. Tang, Z. Yangchun, and Q. Guo, J. Chem. Phys. **135**, 114702 (2011).
[22] C. T. Tzeng, W. S. Lo, J. Y. Yuh, R. Y. Chu, and K. D. Tsuei, Phys. Rev. B **61**, 2263 (2000).
[23] J. K. Gimzewski, S. Modesti, C. Gerber, and R. R. Schlittler, Chem. Phys. Lett. **213**, 401 (1993).
[24] Y. C. Xie, L. Tang, and Q. Guo, Phys. Rev. Lett. **111**, 186101 (2013).
[25] I. Hamada and M. Tsukada, Phys. Rev. B **83**, 245437 (2011).
[26] A. V. Akimov, C. Williams, and A. B. Kolomeisky, J. Phys. Chem. C **116**, 13816 (2012).
[27] X. Torrelles, M. Pedio, C. Cepek, and R. Felici, Phys. Rev. B **86**, 075461 (2012).

[28] A. Fartash, Appl. Phys. Lett. **67**, 3901 (1995).
[29] K. Pussi, H. I. Li, H. Shin, L. N. Serkovic Loli, A. K. Shukla, J. Ledieu, V. Fournée, L. L. Wang, S. Y. Su, K. E. Marino, M. V. Snyder, and R. D. Diehl, Phys. Rev. B **86**, 205406 (2012).
[30] R. van Gastel, E. Somfai, S. B. van Albada, W. van Saarloos, and J. W. M. Frenken, Phys. Rev. Lett. **86**, 1562 (2001).
[31] J. Neugebauer, T. K. Zywietz, M. Scheffler, J. E. Northrup, H. Chen, and R. M. Feenstra, Phys. Rev. Lett. **90**, 056101 (2003).
[32] H. I. Li, K. Pussi, K. J. Hanna, L. L. Wang, D. D. Johnson, H. P. Cheng, H. Shin, S. Curtarolo, W. Moritz, J. A. Smerdon, R. McGrath, and R. D. Diehl, Phys. Rev. Lett. **103**, 056101 (2009).
[33] J. Rundgren, Phys. Rev. B **68**, 125405 (2003).
[34] X. Zhang, W. He, A. Zhao, H. Li, L. Chen, W. W. Pai, J. Hou, M. M. T. Loy, J. Yang, and X. Xiao, Phys. Rev. B **75**, 235444 (2007).
[35] M. Hinterstein, X. Torrelles, R. Felici, J. Rius, M. Huang, S. Fabris, H. Fuess, and M. Pedio, Phys. Rev. B **77**, 153412 (2008).
[36] B. A. Mantooth, E. C. H. Sykes, P. Han, A. M. Moore, Z. J. Donhauser, V. H. Crespi, and P. S. Weiss, J. Phys. Chem. C **111**, 6167 (2007).
[37] See Supplemental Material at http://link.aps.org/supplemental/10.1103/PhysRevB.89.245428 for a complete list of atomic coordinates plus a complete list of R factors, plotted spectra, and experimental and calculated intensities.
[38] X. P. Li, J. P. Lu, and R. M. Martin, Phys. Rev. B **46**, 4301 (1992).
[39] J. P. Lu, X. P. Li, and R. M. Martin, Phys. Rev. Lett. **68**, 1551 (1992).
[40] C. L. Hsu and W. W. Pai, Phys. Rev. B **68**, 245414 (2003).
[41] H. I. Li, G. J. P. Abreu, A. K. Shukla, V. Fournée, J. Ledieu, L. N. Serkovic Loli, S. E. Rauterkus, M. V. Snyder, S. Y. Su, K. E. Marino, and R. D. Diehl, Phys. Rev. B **89**, 085428 (2014).